Biochemical Pharmacology 82 (2011) 2016–2023

Contents lists available at SciVerse ScienceDirect

Biochemical Pharmacology

journal homepage: www.elsevier.com/locate/biochempharm

Homodimerization of UDP-glucuronosyltransferase 2B7 (UGT2B7) and identification of a putative dimerization domain by protein homology modeling

Benjamin C. Lewis, Peter I. Mackenzie, John O. Miners *

Department of Clinical Pharmacology, School of Medicine, Flinders University, Adelaide, Australia

ARTICLE INFO

Article history:
Received 1 July 2011
Received in revised form 5 September 2011
Accepted 6 September 2011
Available online 14 September 2011

Keywords:
UDP-glucuronosyltransferase
UGT2B7
Homology model
Dimerization
Enzyme kinetics
Glucuronidation

ABSTRACT

Although homodimerization of UGT1A proteins is well established, direct evidence for dimerization of UGT2B7, which is arguably the most important enzyme involved in human drug glucuronidation, is currently lacking. This study characterized UGT2B7 homodimerization by co-immunopreciptation and generated a UGT2B7 homology model that identified the dimerization domain. It was demonstrated that co-expressed, solubilized UGT2B7 proteins differentially tagged with hemagglutinin (UGT2B7-HA) and c-MYC (UGT2B7-cMYC) co-immunoprecipitated as active homodimers that catalyzed 4-methylumbelliferone glucuronidation. Substrate binding affinities (assessed as S_{50} values) of the tagged and co-expressed tagged proteins were essentially identical to that of native UGT2B7. Co-association was not observed in a 'mixed' UGT2B7-HA and UGT2B7-cMYC protein preparation. Generation of a UGT2B7 homology model established from plant and human templates was achieved using SYBYLX1.2 with all residues energy minimized using the Tripos Force Field. The UGT2B7 model allowed elucidation of a putative protein dimerization domain within the B′–C loop of each UGT2B7 monomer. The eighteen amino acid dimerization domain is present in all UGT2B enzymes and comprises a proposed dimerization signature motif (FPPSYVPVVMS). Stabilization of the dimer interface is maintained by the formation of two salt bridges, aromatic π–π stacking interactions, two S-aromatic (face) interactions, and the presence of 'proline brackets'. The homology model further provides important insights into structure–function relationships of this enzyme and the mechanism responsible for the atypical glucuronidation kinetics for substrates of UGT2B7 and other human UGT enzymes.

1. Introduction

The UDP-glucuronosyltransferases (UGT) comprise a superfamily of membrane bound enzymes that catalyze the conjugation of glucuronic acid, derived from UDP-glucuronic acid (UDPGA), to typically lipophilic substrates bearing a suitable nucleophilic acceptor functional group. The glucuronidation reaction provides a clearance and detoxification mechanism for drugs from all therapeutic classes, environmental chemicals, and endogenous compounds that include bilirubin, fatty acids, and steroid hormones [1,2]. Eighteen functional human UGT enzymes that utilize UDPGA as cofactor have been identified to date, and these have been classified in three subfamilies (UGT1A, UGT2A and UGT2B) based on amino acid sequence identity [3]. The individual UGT enzymes exhibit distinct, but frequently overlapping, substrate selectivities [4,5].

There is accumulating evidence that UGT enzymes exist as oligomers in homodimeric and heterodimeric states [6]. Gel permeation chromatography, cross-linking studies and two-hybrid analysis in yeast and mammalian systems were employed to demonstrate homodimerization of UGT1A1 [7]. In addition to UGT1A1, fluorescence resonance energy transfer (FRET) [8] and co-immunoprecipitation (Co-IP) [8,9] studies have provided evidence of homodimerization of other UGT1A subfamily proteins (viz. UGT 1A3, 1A4, 1A6, 1A7, 1A8, 1A9 and 1A10). While definitive studies with human UGT2A and UGT2B enzymes are lacking, it has been reported that co-expression of two inactive forms of rat UGT2B1 resulted in restoration of catalytic activity, consistent with functional dimerization [10].

Multiple lines of evidence similarly suggest the occurrence of heterodimerization. FRET and Co-IP data indicated that UGT1A1 may heterodimerize with UGT 1A3, 1A4, 1A6, 1A7, 1A8, 1A9 and 1A10 [8], although two-hybrid analysis did not identify an association between UGT1A1 and UGT1A6 [7]. Consistent with protein–protein interactions, altered enzyme activity and thermal stability have been demonstrated following co-expression of various human UGT1A proteins [11–14] and co-expression of UGT2B7 and UGT1A proteins [15]. Co-expression of guinea pig UGT2B21 and

* Corresponding author at: Department of Clinical Pharmacology, Flinders University School of Medicine, Flinders Medical Centre, Bedford Park, SA 5042, Australia. Tel.: +61 8 8204 4131; fax: +61 8 8204 5114.
E-mail address: john.miners@flinders.edu.au (J.O. Miners).

0006-2952/$ – see front matter © 2011 Elsevier Inc. All rights reserved.
doi:10.1016/j.bcp.2011.09.007

UGT2B22 similarly resulted in the altered glucuronidation of chloramphenicol and morphine [16,17], while immunopurification and chemical cross-linking studies are suggestive of interactions between rat UGT2B1 and UGT1A proteins [18].

UGT2B7 is arguably the most important enzyme involved in drug glucuronidation [2,19]. For example, UGT2B7 contributes to the glucuronidation of opioids, including codeine and morphine [20–22], anti-cancer agents [23,24], gemfibrozil [25], valproic acid [26], zidovudine [20], and non-steroidal anti-inflammatory agents [26,27]. Furthermore, UGT2B7 glucuronidates the mineralocorticoid aldosterone and other C19 and C21 hydroxy-steroids [28–30]. Data from kinetic and inhibition studies along with the presence of bands corresponding to the molecular weights of oligomeric species on western blots suggests that UGT2B7 may exist as a homodimer [15,31–33], but direct evidence for homodimerization is currently lacking.

The aim of the present study was to investigate homodimerization of UGT2B7. Following demonstration of a direct protein–protein interaction by Co-IP, a homology model that identified the dimerisation domain was generated based on the X-ray crystal coordinates of the C-terminal region of human UGT2B7 [34] and several plant glycosyltransferases.

2. Materials and methods

2.1. Chemicals and reagents

4-Methylumbelliferone (4MU), 4-methylumbelliferone β-D-glucuronide (4MUG), and UDP-glucuronic acid trisodium salt (UDPGA) were purchased from Sigma–Aldrich (Sydney, Australia); *Pfu* Ultra II HS Polymerase from Stratagene (La Jolla, CA, USA); Shrimp Alkaline Phosphatase from Roche Diagnostics GmbH (Penzbeg, Germany); restriction enzymes were from New England Biolabs (Ipswich, MA, USA); Dulbecco's modified Eagle's medium (DMEM), MEM non-essential amino acids solution (10 mM; ×100), and penicillin/streptomycin solution (penicillin-G 5000 U/mL – streptomycin sulfate 5000 mg/mL) from Invitrogen (Carlsbad, CA, USA). Other reagents and solvents were of analytical reagent grade.

2.2. Human liver microsomes (HLM)

HLM were used as both positive and negative antibody controls in western blots. Human liver tissue was obtained from the human liver 'bank' of the Department of Clinical Pharmacology, Flinders Medical Centre. Approval for the use of human liver tissue in xenobiotic metabolism studies was obtained from the Flinders Medical Centre Research Ethics Committee. HLM were prepared from five livers (H7, H10, H15, H29 and H40) by differential centrifugation [27]. Pooled HLM were prepared by mixing equal amounts of individual microsomal preparations.

2.3. UGT2B7 cDNA, tagging, cloning, and expression

The human UGT2B7 cDNA was isolated as reported previously [26], differentially tagged on the C-terminus with either hemagglutinin (HA; YPYDVPDYA) or cMYC (EQKLISEEDL), then shuttled into the pEF-IRES(5) mammalian expression vector. Cells were individually transfected with untagged UGT2B7 and the tagged UGT2B7-HA and UGT2B7-cMYC expression constructs, and co-transfected with UGT2B7-HA and UGT2B7-cMYC (UGT2B7-HA + cMYC). All transfections were conducted with equal total amounts of expression construct (4 μg) using Lipofectamine2000 and OptiMEM (Invitrogen, CA, USA). The stable expression of UGT2B7-WT, UGT2B7-HA, UGT2B7-cMYC, and co-expressed UGT2B7-HA + cMYC was achieved in the human embryonic kidney cell line HEK293 T according to a published procedure [32].

2.4. Co-immunoprecipitation of expressed UGT2B7 proteins

Harvested cells were solubilized on ice for 2 h in solubilization buffer (0.5% NP-40, 0.25% sodium deoxycholate, 50 mM Tris–HCl; pH 7.5, 150 mM NaCl, 1 mM EDTA) containing 1% protease inhibitors (Roche Diagnostics GmbH, Mannheim Germany). Following centrifugation at 15,000 × *g* for 30 min at 4 °C the supernatant fraction (200 μg) was diluted in ice cold solubilizing buffer to a final volume of 500 μL, then 50 μL of anti-HA Affinity Matrix (Roche Diagnostics GmbH, Mannheim Germany) was added. Samples were incubated overnight at 4 °C on a rocking platform to allow for the co-precipitation of protein complexes and then centrifuged (13,000 × *g* for 1 min at 4 °C) to pellet the anti-HA affinity matrix. The pellet was washed with solubilization buffer (3 × 1 mL) and the matrix resuspended in electrophoresis sample buffer (250 mM Tris-base; pH 6.8, 50% (v/v) glycerol, 5% (w/v) SDS, 0.2% (w/v) bromophenol blue, 250 mM DTT).

2.5. Immunoblotting

Denatured proteins from each Co-IP reaction were loaded onto 4–10% PAGE gels, separated (170 V), and then rectilinearly transferred to Trans-Blot® Transfer Medium pure nitrocellulose (BIORAD; 0.45 μm; 90 V). Immuno-detection of UGT2B7 proteins was achieved by probing blots with anti-HA (US Biological, MA, USA), anti-cMYC (Rockland, PA, USA), and anti-UGT2B7 [35] primary antibodies (1:3000 dilution) with ImmunoPure® Goat anti-Rabbit IgG used as the secondary antibody (H + L; peroxidase conjugated; Rockford, IL, USA) (1:4000 dilution). Immunoreactivity was detected using the BM Chemiluminescence Blotting Substrate (Roche Diagnostics GmbH, Mannheim Germany) and recorded digitally using the FUJIFILM LAS-400 image reader (version 2.0; FUJIFILM Life Science Corporation; Tokyo, Japan).

2.6. Measurement of 4-MU glucuronidation

4-MUG formation was determined in opaque glass tubes at 37 °C in a total incubation volume of 0.2 mL. Incubation mixtures contained HEK293 T cell lysate expressing recombinant UGT2B7 (1 mg/mL), phosphate buffer (0.1 M, pH 7.4), $MgCl_2$ (4 mM), UDPGA (5 mM), and 4-MU (25–1500 μM). Following a 5 min pre-incubation at 37 °C, reactions were initiated by the addition of cofactor (UDPGA). Incubations were terminated after 90 min by the addition of 2.0 μL of ice cold perchloric acid (70%). Reaction mixtures were vortex mixed, cooled on ice for 10 min, centrifuged (5000 × *g* for 10 min at 4 °C), and an aliquot of the supernatant fraction (40 μL) injected onto the HPLC column.

4-MUG was separated using a Waters Nova-Pak® C18 column (150 × 3.9 mm, 4 μm; Waters Corporation, MA, USA). The mobile phase consisted of 10 mM triethylamine (TEA) adjusted to pH 2.5 with 70% perchloric acid (phase A) and acetonitrile (phase B). Initial conditions were 96% A held for 3.0 min, after which time the composition was changed to 70% A/30% B over 0.1 min and then held for 1.0 min. The mobile phase was returned to initial conditions over 0.1 min and then held for 3.8 min before injecting the next sample. 4-MUG was monitored by UV detection at 316 nm. The retention time of 4-MUG was 3.5 min using a mobile phase flow rate of 1.0 mL/min. Unknown concentrations of 4-MUG were determined by comparison of the peak area to a calibration curve constructed in the concentration range 1–10 μM.

2.7. Calculation of 4-MU glucuronidation kinetic parameters

All 4-MU activities represent the mean of duplicate estimates (<10% variance). Rates of 4-MUG formation over the substrate concentration range (25–1500 μM) were fit with the Hill equation

(see below) using the non-linear curve fitting program EnzFitter (Biosoft, Cambridge, UK) to generate kinetic constants (S_{50}, V_{max}, and n) for 4-MU glucuronidation by UGT2B7 and the individually tagged proteins:

$$v = \frac{V_{max}[S]^n}{{S_{50}}^n + [S]^n}$$

where v is the rate of reaction (rate of metabolite formation), V_{max} is the maximal velocity, S is the substrate concentration, S_{50} is the substrate concentration at 1/2 V_{max}, and n is the Hill coefficient.

2.8. In silico modeling of UGT2B7

A homology model of human UGT2B7 was constructed using FUGUE and ORCHESTRAR (SYBYL-X 1.2, Tripos™). The homologs identified by FUGUE were refined against profile Hidden Markov Model [36] data constructed from the human UGT2B7 coding sequence (CDS). The crystal templates of grape UDP-glucose flavanoid 3-*O* glucosyltransferase (2C1X, 2C1Z, 2C9Z), barrel medic UDP-glucose flavanoid/triterpene glucosyltransferase UGT71G1 (2ACV, 2ACW), and the cofactor-binding domain of UGT2B7 (2O6L) [34] were obtained from the Brookhaven Protein Data Bank (PDB). The highest acceptable inter-Cα distance between equivalent residues within a sequence conserved region was 1.5 Å, with a RMS difference of 0.00001 Å considered significant. Loops not modeled were found by loop threading all crystal structures of the HOMSTRAD database (SYBYL-X 1.2, Tripos™). Refinement of the UGT2B7 model was achieved using the method described by Lewis et al. [37]. Briefly, main-chain and side-chain torsions were independently minimized using the conjugate-gradient method reported by Powell [38], and then the model was minimized as a whole.

3. Results

3.1. Expression of UGT2B7 and tagged UGT2B7 proteins

UGT2B7, UGT2B7-HA, UGT2B7-cMYC, and co-expressed UGT2B7-HA + cMYC proteins were expressed in HEK293T cells. Cell lysates were screened for the presence of UGT2B7 protein by immunoblotting using a UGT2B7 specific antibody (Fig. 1A). Expression levels of UGT2B7-HA, UGT2B7-cMYC, and co-expressed UGT2B7-HA + cMYC relative to wild-type were 30.3 ± 1%, 23.8 ± 1.2%, and 18.4 ± 0.6% (mean ± SD of 3 measurements), respectively (Fig. 1A). Lysates probed with anti-HA antibody revealed immunoreactivity with UGT2B7-HA and co-expressed UGT2B7-HA + cMYC proteins only (Fig. 1B). The intensity of the HA-tagged protein in the co-expressed UGT2B7-HA + cMYC sample was approximately half that of individually expressed UGT2B7-HA. This result is consistent with the amount of the individual constructs transfected in the co-expressed sample (2 μg UGT2B7-HA, 2 μg UGT2B7-cMYC). Lysates probed with the anti-cMYC antibody demonstrated immunoreactivity with UGT2B7-cMYC and co-expressed UGT2B7-HA + cMYC proteins in addition to a glutathione cMYC tagged positive control (GST-cMYC) (Fig. 1C). As expected, approximately half of the cMYC-tagged protein intensity was observed in the co-expressed UGT2B7-HA + cMYC sample compared to the UGT2B7-cMYC alone.

3.2. Kinetics of 4-MU glucuronidation by UGT2B7 and the tagged UGT2B7 proteins

UGT2B7 and the tagged UGT2B7-HA, UGT2B7-cMYC, and co-expressed UGT2B7-HA + cMYC proteins catalyzed 4-MU glucuronidation. All enzymes exhibited sigmoidal kinetics and data were well modeled by the Hill equation (Fig. 2, Table 1). V_{max} values reported in Table 1 were normalized for expression relative to wild-type UGT2B7 based on densitometry (Section 3.1). The kinetic parameters for 4-MU glucuronidation by untagged UGT2B7 (S_{50} 522 ± 21 μM, V_{max} 246 ± 6.8 pmol/min/mg, n = 1.8) are similar to previous data from this laboratory [32,33]. The individually expressed UGT2B7-HA and UGT2B7-cMYC enzymes displayed S_{50} values that were essentially identical to those of the wild-type UGT2B7. Likewise, cooperativity (as measured by the Hill coefficient) was consistent among all UGT2B7 proteins, untagged and tagged (Table 1). Taken together with the similar S_{50} values, these data suggest that substrate binding and enzyme protein conformation are unaffected by tagging with HA and cMYC. However, V_{max} values differed even after correction for relative expression. The tagged enzymes exhibited V_{max} values that were approximately 7-fold lower than UGT2B7 indicating that the HA and cMYC C-terminal tags had a significant effect on catalytic efficiency. The 'tag' effect on V_{max} was also observed with the co-expressed UGT2B7-HA + cMYC enzyme preparation, which exhibited a 70% decrease in V_{max} relative to the wild-type (Table 1).

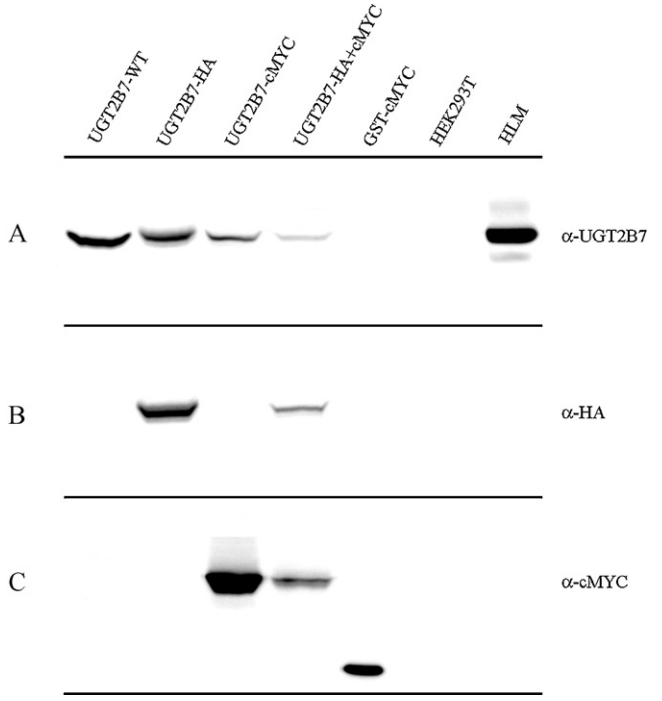

Fig. 1. Immunoblot of wild-type and tagged UGT2B7 proteins. HEK293T cell lysate (50 μg) expressing the protein of interest was resolved by SDS-PAGE, blotted to nitrocellulose, and probed separately with: (A) anti-UGT2B7, (B) anti-HA, and (C) anti-cMYC antiserum. Wild-type UGT2B7 (lane 1), UGT2B7-HA (lane 2), UGT2B7-cMYC (lane 3), co-expressed UGT2B7-HA + cMYC (lane 4), GST-cMYC control (lane 5), vector control HEK293T cell lysate (lane 6), and human liver microsomes (lane 7). The immuno-reactive bands occur at 60 kDa.

Table 1
Derived kinetic parameters for 4-MU glucuronidation by wild-type and tagged UGT2B7.

Enzyme	S_{50}[a] (μM)	V_{max}[a] (pmol/min/mg)	Normalized V_{max}[b] (pmol/min/mg)	Hill coefficient
UGT2B7-WT	522 ± 21	246 ± 6.8	246	1.8
UGT2B7-HA	508 ± 7	11 ± 0.1	36	1.8
UGT2B7-cMYC	496 ± 24	8 ± 0.3	33	1.8
UGT2B7-HA + cMYC	497 ± 34	15 ± 0.7	81	1.8

[a] Data are shown as the parameter ± S.E. of the parameter fit.
[b] V_{max} values normalized for expression relative to wild-type UGT2B7.

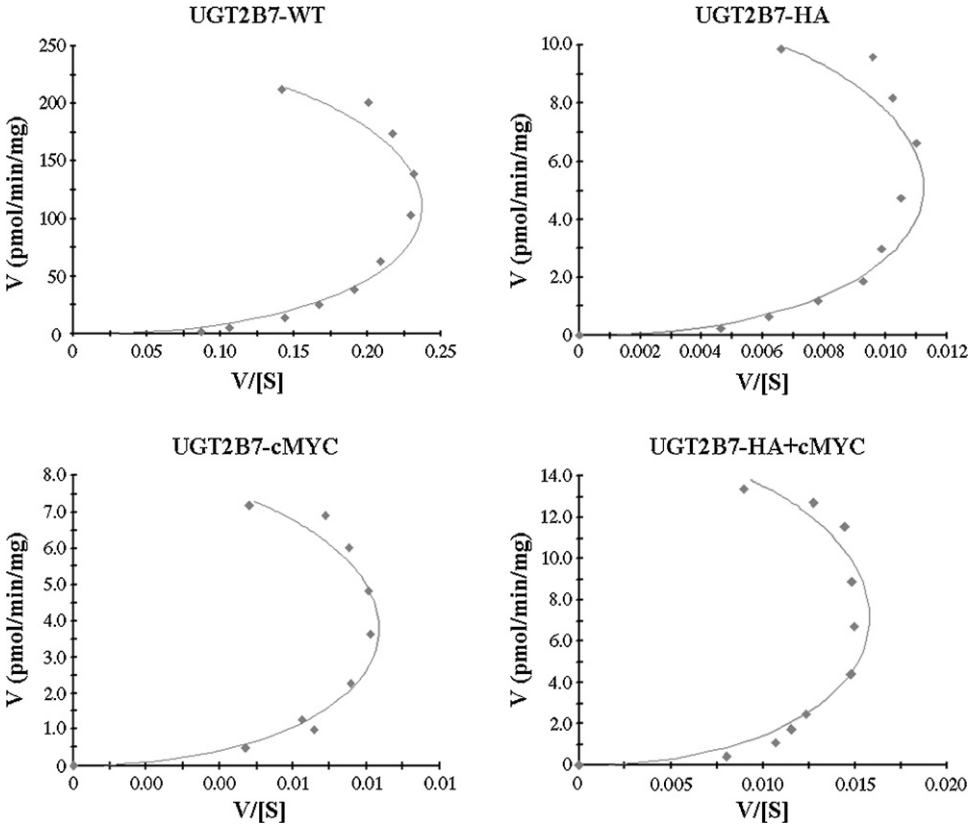

Fig. 2. Representative Eadie–Hofstee plots for 4-MU glucuronidation by wild-type UGT2B7, UGT2B7-HA, UGT2B7-cMYC, and co-expressed UGT2B7-HA + cMYC. Data points are the average (<10% variance) of duplicate measurements. Curves are from fitting with the Hill equation using EnzFitter (Biosoft, Cambridge, UK).

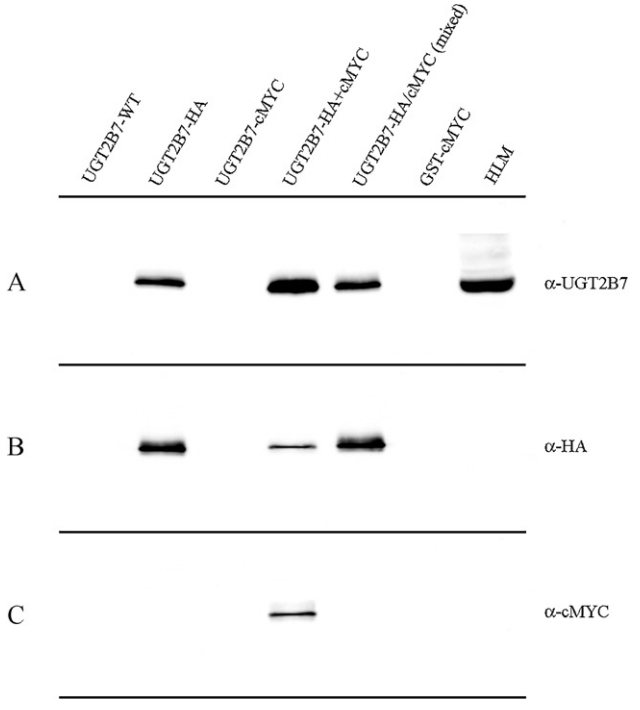

Fig. 3. Immunoblot of co-immunoprecipitated wild-type and tagged UGT2B7 proteins. Co-IP products were blotted to nitrocellulose, and probed separately with: (A) anti-UGT2B7, (B) anti-HA, and (C) anti-cMYC antiserum. Wild-type UGT2B7 (lane 1), UGT2B7-HA (lane 2), UGT2B7-cMYC (lane 3), co-expressed UGT2B7-HA + cMYC (lane 4), mixed UGT2B7-HA/cMYC (lane 5), GST-cMYC control (lane 6), and human liver microsomes (lane 7). Immuno-reactive bands are present at 60 kDa.

3.3. Co-immunoprecipitation and homodimerization of UGT2B7

Co-IP of solubilized protein was performed with an anti-HA affinity matrix. Western blotting using the anti-UGT2B7 specific antibody revealed that after Co-IP of solubilized proteins UGT2B7 is only present in those samples that contain HA-conjugated UGT2B7 (i.e. UGT2B7-HA, co-expressed UGT2B7-HA + cMYC, and a control sample containing a mixture of UGT2B7-HA and UGT2B7-cMYC; UGT2B7-HA/cMYC, 25 μg each) (Fig. 3A). Band intensities were equivalent for all samples, including the co-expressed UGT2B7-HA + cMYC, as the anti-UGT2B7 specific antibody detects total UGT2B7, independent of tag type. When probed with the anti-HA antibody, HA-conjugated UGT2B7 was observed in UGT2B7-HA, co-expressed UGT2B7-HA + cMYC, and mixed UGT2B7-HA/cMYC samples (Fig. 3B). Detection with this antibody revealed a band intensity for the co-expressed UGT2B7-HA + cMYC of approximately half that of the UGT2B7-HA sample which, again, corresponds to the relative amount of the transfected construct. Co-IP samples were further probed with the anti-cMYC antibody. cMYC conjugated UGT2B7 protein was observed only in the co-expressed UGT2B7-HA + cMYC sample (Fig. 3C). The band intensity of this sample is similar to the co-expressed UGT2B7-HA + cMYC sample probed with anti-HA antibody (Fig. 3B). The absence of cMYC conjugated UGT2B7 in the UGT2B7-cMYC sample is consistent with the lack of binding of this protein to the anti-HA affinity matrix. Moreover, no bands were observed for the UGT2B7-HA/cMYC mixture after Co-IP. Co-IP data were confirmed in three independent experiments.

3.4. In silico modeling of UGT2B7

Inspection of the UGT2B7 homology model revealed eleven α-helices and nine β-sheets, designated A-K and 1–9, respectively. Four additional helices, A′, B′, C′, and F′, are also present. The

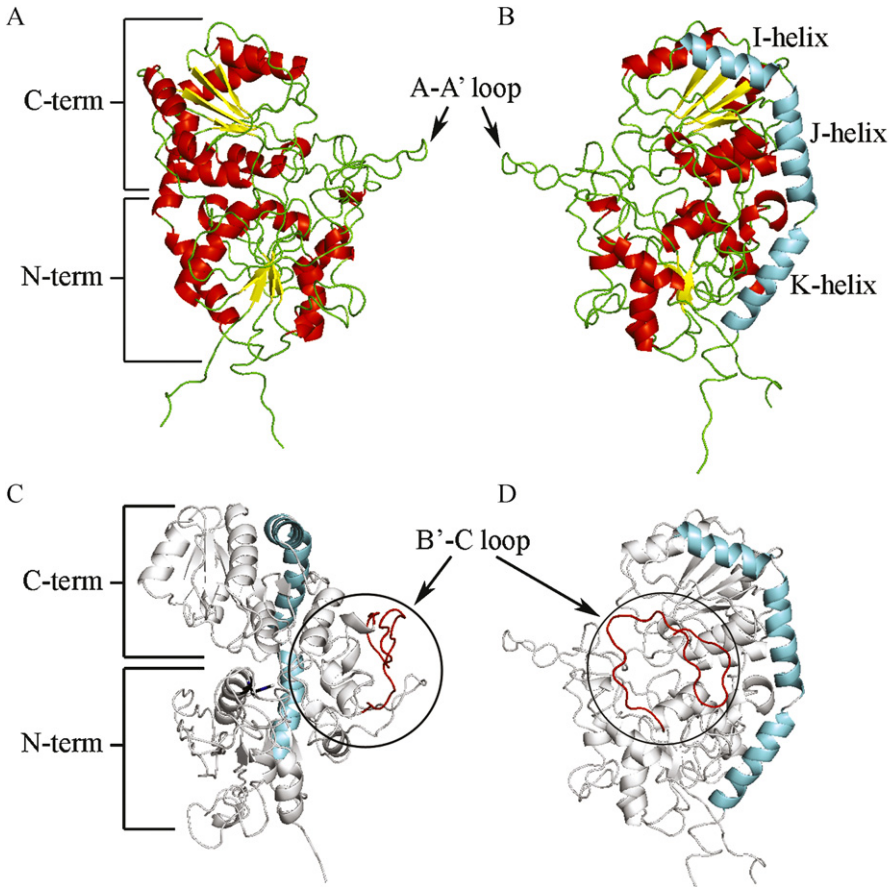

Fig. 4. The tertiary organization of the UGT2B7 homology mode. (Panel A) The catalytic N-terminal domain is coupled to the cofactor binding domain of the C-terminus via helices I, J, and K and the A–A′ loop (Panel B). A third smaller domain (Panel C; circle), separate to the catalytic domains, encompasses hydrophobic residues of the B′–C loop (Panel D; circle).

tertiary organization of UGT2B7 (Fig. 4A) shows close resemblance to the crystallized templates when each structure is overlaid. However, this is not reflected in calculated RMSD values (2O61; 1.9 Å, 2ACV; 9.7 Å, 2C1X; 10.0 Å) and is primarily due to the large sequence variability in the N-terminus. The solvent accessible surface area of UGT2B7 was calculated as 21021 $Å^2$ with a total energy (−622.64 kcal/mol), which is comparable to the crystal templates comprising the entire protein (2O61; −215.6, 2ACV; −730.7, 2C1X; −670.9 kcal/mol). The protein exists as two main catalytic domains 'hinged' together by the I, J, and K helices with a large flexible A–A′ loop region (Fig. 4B). A third, smaller domain (Fig. 4C) that is separate to the catalytic domains encompasses the hydrophobic B′–C loop region (Fig. 4D).

3.5. UGT2B7 putative dimerization domain

The cluster of highly hydrophobic amino acids on the surface of the UGT2B7 model (within the B′–C loop domain) was identified as the putative protein dimerization domain. The protein–protein interaction site spans residues 183 through 200 of the N-terminus (Fig. 5A). The eighteen amino acid putative dimerization domain is present in all UGT2B enzymes (Fig. 6), and includes the signature motif FPPSYVPVVMS (residues 189–199; Fig. 6 box). The UGT2B7 dimerization domain was verified using the InterProSurf protein–protein interaction server (http://curie.utmb.edu/), which identified 50% of all residues. The predicted region encompasses residues 187–195 and includes proline residues at positions 190 and 195, which function as 'proline brackets'. Proline residues in this type of arrangement are characteristically found in the flanking segments of protein–protein interaction sites [39]. In addition to the 'proline brackets', histidine 183, phenylalanines 187 and 189, methionine 198, and glutamate 200 of UGT2B7 all potentially aid association at the dimer interface (Fig. 5B). Inspection of the in silico dimer (Fig. 5B and C) reveals H183 can form a monodentate salt bridge [40] with E200 of its complementary protein monomer. In addition, a symmetrical quartet of face-to-face π–π interactions is generated by the interaction between F187 in each of the complementary monomers, and by the interaction between F189 in each complementary monomer (Fig. 5C) [41]. Further stabilization of the dimer interface occurs due to the interaction between the sulfur atoms of M198 with the aromatic face of F187 (Fig. 5C). Here, the sulfur atom behaves as an electrophile and the ring as a nucleophile [42]. Thus, five key interactions spanning the dimerization domain potentially stabilize the dimer interface.

4. Discussion

Although homodimerization of UGT1A enzymes has been demonstrated [6–9], evidence for human UGT2B subfamily enzymes is limited. Furthermore, the mechanism of UGT dimerization and the residues that comprise the dimer interface have not been elucidated. Here, Co-IP experiments with HA- and cMYC-tagged proteins demonstrated that human UGT2B7, which is arguably the most important UGT enzyme involved in drug metabolism, forms catalytically active homodimers with the ability to catalyze 4-MU glucuronidation (Fig. 2). Monomer association was confirmed by the detection of cMYC tagged UGT2B7 in the co-expressed UGT2B7-HA + cMYC protein preparation subjected to HA affinity chromatography, but not in the 'mixed' UGT2B7-HA/cMYC protein preparation. The latter observation precludes the non-specific aggregation of

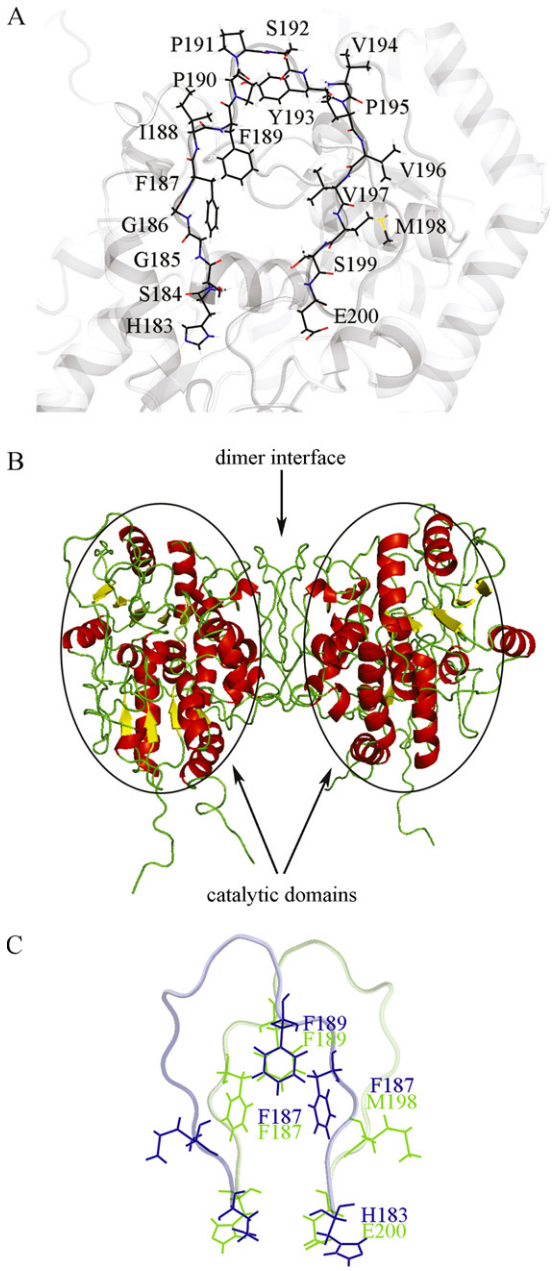

Fig. 5. Structural organization of dimeric human UGT2B7. The hydrophobic UGT2B7 putative dimerization domain encompasses residues 183–200 (Panel A). Panel B shows the protein–protein interaction at the dimer interface. Stabilization at the dimer interface (Panel C) is maintained by the formation of two salt bridges (H183/E200), aromatic π–π stacking interactions (F187/F187, F189/F189), and two S-aromatic (face) interactions (F187/M198).

Fig. 6. Sequence alignment of the putative dimerization domains of human UGT2B enzymes. The dimerization domain encompasses residues 183 through 200, which incorporates the highly conserved UGT2B family dimerization signature motif (boxed residues).

UGT2B7 proteins as a basis for co-precipitation or cross linking. The Co-IP data presented here are consistent with the observation of bands corresponding to the molecular weights of monomeric and dimeric UGT2B7 using non-denaturing PAGE [15].

Kinetic data generated with UGT2B7 as the enzyme source provide functional evidence for protein homodimerization. 4-MU glucuronidation by UGT2B7 exhibits sigmoidal kinetics which may be analyzed by multi-site models that assume the existence of two equivalent, interacting binding sites [32,33]. The kinetics of morphine and 1-naphthol (1-NP) glucuronidation by UGT2B7 similarly suggest the occurrence of two equivalent binding sites [21,32,33]. Furthermore, the effects of 4-MU and 1-NP on zidovudine glucuronidation by UGT2B7 were well described by a two-substrate binding site model in which there is no interaction between the sites in the absence of 'modifier', but heterotrophic co-operativity results from the binding of 4-MU or 1-NP [33]. It may be speculated that the two equivalent binding sites assumed in these models arises from homodimerization. Indeed, 'atypical' (i.e. non-hyperbolic) glucuronidation kinetics is also a feature of several of the UGT1A subfamily enzymes known to form homodimers and multi-site kinetic modeling has been successfully applied to these reactions [33,43].

A UGT2B7 homology model was generated to identify the dimerization domain. The model demonstrated the presence of a structural domain that encompasses the B′–C loop. This domain acts independently of the 'hinged' N-terminal and C-terminal domains (Fig. 4B and C) and comprises largely hydrophobic surface residues between positions 183 and 200 (Fig. 5A). The presence of such a hydrophobic region on the surface of the protein is highly suggestive of a protein–protein interaction site. Further evidence for the proposed dimerization interface comes from residue propensities (favorable physicochemical tendencies), size, shape, solvent accessibility, residue pairing preferences, and the presence of 'proline brackets' [42,44–48]. Short segments of 3–7 amino acids flanked by 'proline brackets' are commonly found in protein–protein interaction sites and are known to enhance the interaction between monomers [42] and play an important role in molecular recognition. When two UGT2B7 monomers are aligned in silico to generate the homodimer (Fig. 5B), it is evident that the 'proline brackets' block the continuation of neighboring secondary structures into the dimer interaction site and protects the conformational integrity of the putative dimerization domain [42]. Further geometric constraint of the dimerization domain arises from extensive Cβ-branching (Fig. 6). Additional stabilization at the dimer interface is maintained by the formation of two salt bridges, aromatic π–π stacking interactions, and two S-aromatic (face) interactions (Fig. 5C).

The dimerization signature motif identified (FPPSYVPVVMS) is highly conserved in all human UGT2B enzymes with 100% identity observed in UGT2B4, UGT2B7, UGT2B10, UGT2B15, and UGT2B17. Valine is substituted for isoleucine at positions 194 and 196 in UGT2B11 and at residue 194 in UGT2B28 (Fig. 6). The conserved isoleucine substitution at these positions maintains the rigid backbone architecture of the protein dimerization domain through Cβ-branching. The presence of this domain indicates that human UGT2B proteins can potentially form both hetero- and homodimers. The analogous region in UGT1A family enzymes also contains the dimerization signature motif (PXPXSYVPXXX), consistent with heterodimerization of UGT1A and UGT2B proteins. Interactions between UGT1A and UGT2B enzymes have been suggested by a number of studies [15,18]. Moreover, the dimerization signature motif is not exclusive to human UGT enzymes. The UGT2B dimerization signature motif is present in the rat UGT2B1 protein (XPPSYVPVVXX), which has been reported to form catalytically active homodimers [10]. It is noteworthy that the eleven amino acid dimerization signature motif of each

vertebrate UGT family differs slightly, but the core PXSYVP sequence containing the proline 'brackets' is entirely conserved across all vertebrates (data not shown).

The stability of numerous dimeric proteins has been measured by equilibrium denaturation experiments, with results revealing two types of equilibrium transition states in the formation of dimers [49]; a 2-state transition, which comprises an active dimer state and a denatured monomer state and a 3-state transition, which comprises an active dimer state, a stable monomer state, and a denatured monomer state. Those monomers that maintain the same structural conformation as found in the dimeric state belong to a 'rigid body' mode of 3-state binding. The alternative to the 'rigid body' mode of monomer binding occurs when the structural conformation of the monomer varies from that in the dimer [50]. Based on the strongly hydrophobic nature of the UGT2B putative dimerization domain, it is unlikely monomer binding follows the 'rigid body' mode of 3-state binding, but rather exists as either a 2-state or 3-state binder with deviation in the structural conformation of the monomer.

Evidence that UGT2B7 adopts a 2-state binding transition can be inferred from previous chimeragenesis experiments conducted in this laboratory [31], which generated hybrid UGT2B7 and UGT2B15 proteins using variable lengths of the coding region that spanned residues 61–197. This region incorporates the variable A–A′ loop and the B′–C loop domains, the latter comprising the UGT2B7 dimerization domain identified here. Results showed that glucuronidation of 4-MU by wild-type UGT2B7 exhibits sigmoidal kinetics consistent with the simultaneous binding of two substrate molecules in the active-site, similar to data reported in this study (Table 1). Substitution of the UGT2B7 A–A′ loop and B′–C loop domains with those of UGT2B15 induced a switch to hyperbolic (Michaelis–Menten) kinetics, characteristic of 4-MU glucuronidation by wild-type UGT2B15 [31]. Further experiments showed that all UGT2B7 chimeras containing the UGT2B15 dimerization domain were inactive unless they included the full complementary UGT2B15 A–A′ loop and B′–C loop domains. Based on previous data [31], it would appear that UGT2B7 Exhibits 2-state transition binding where catalytic activity is potentially dependant on successful dimerization. However, it is emphasized that complementarity is also required between the putative dimerization domain and any adjacent neighboring secondary structure. This implies that the inactive UGT2B7-15 chimeras exist in the denatured monomer state, with structural distortions at the unshielded hydrophobic dimerization domain.

In summary, identification of the association of two differentially tagged UGT2B7 monomers has confirmed the homodimerization of UGT2B7. Generation of a UGT2B7 homology model permitted elucidation of the residues that potentially comprise the dimer interface, the UGT2B putative dimerization domain, and the core UGT dimerization signature motif present in all vertebrates. Furthermore, the homology model provides important insights into the structure–activity relationships of this enzyme and the mechanism responsible for the atypical glucuronidation kinetics of substrates for UGT2B7 and other human UGT enzymes.

Acknowledgement

This study was supported by a research project grant from the National Health and Medical Research Council of Australia.

References

[1] Miners JO, Mackenzie PI. Drug glucuronidation in humans. Pharmacol Ther 1991;51:347–69.
[2] Kiang TKL, Ensom MHH, Chang TKH. UDP-glucuronosyltransferases and clinical drug-drug interactions. Pharmacol Ther 2005;106:97–132.
[3] Mackenzie PI, Bock KW, Burchell B, Guillemette C, Ikushiro S, Iyanagi T, et al. Nomenclature update for the mammalian UDP-glucuronosyltransferase (UGT) gene family. Pharmacogenet Genom 2005;15:677–85.
[4] Miners JO, Smith PA, Sorich MJ, McKinnon RA, Mackenzie PI. Predicting human drug glucuronidation: application of in vitro and in silico modeling approaches. Annu Rev Pharmacol Toxicol 2004;44:1–25.
[5] Miners JO, Knights KM, Houston JB, Mackenzie PI. In vitro–in vivo correlation for drugs and other compounds eliminated by glucuronidation in humans: pitfalls and promises. Biochem Pharmacol 2006;71:1531–9.
[6] Finel M, Kurkela M, The. UDP-glucuronosyltransferases as oligomeric enzymes. Curr Drug Metab 2008;9:70–6.
[7] Ghosh SS, Sappal BS, Kalpana GV, Lee SW, Chowdhury JR, Chowdhury NR. Homodimerization of human bilirubin-uridine-diphosphoglucuronate glucuronosyltransferase-1 (UGT1A1) and its functional implications. J Biol Chem 2001;276:42108–15.
[8] Operana TN, Tukey RH. Oligomerization of the UDP-glucuronosyltransferase 1A proteins – Homo- and hetero-dimerization analysis by fluorescence resonance energy transfer and co-immunoprecipitation. J Biol Chem 2007;282:4821–9.
[9] Kurkela M, Garcia-Horsman JA, Luukanen L, Morsky S, Taskinen J, Baumann J, et al. Expression and characterization of recombinant human UDP-glucuronosyltransferases (UGTs). UGT1A9 is more resistant to detergent inhibition than the other UGTs and was purified as an active dimeric enzyme. J Biol Chem 2003;278:3536–44.
[10] Meech R, Mackenzie PI. UDP-glucuronosyltransferase, the role of the amino terminus in dimerization. J Biol Chem 1997;272:26913–7.
[11] Kurkela M, Hirvonen J, Kostiainen R, Finel M. The interactions between the N-terminal and C-terminal domains of the human UDP-glucuronosyltransferases are partly isoform-specific, and may involve both monomers. Biochem Pharmacol 2004;68:2443–50.
[12] Fujiwara R, Nakajima M, Yamanaka H, Katoh M, Yokoi T. Interactions between UGT1A1, UGT1A4, and UGT1A6 affect their enzymatic activities. Drug Metab Dispos 2007;35:1781–7.
[13] Fujiwara R, Nakajima M, Yamanaka H, Nakamura A, Katoh M, Ikushiro S-I, et al. Effects of coexpression of UGT1A9 on enzymatic activities of human UGT1A enzymes. Drug Metab Dispos 2007;35:747–57.
[14] Nakajima M, Yamanaka H, Fujiwara R, Katoh M, Yokoi T. Stereoselective glucuronidation of 5-(4′-hydroxyphenyl)-5-phenylhydantoin by human UDP-glucuronosyltransferase (UGT) 1A1, UGT1A9, and UGT2B15: effects of UGT–UGT interactions. Drug Metab Dispos 2007;35:1679–86.
[15] Fujiwara R, Nakajima M, Oda S, Yamanaka H, Ikushiro S-I, Sakai T, et al. Interactions between human UDP-glucuronosyltransferase (UGT) 2B7 and UGT1A enzymes. J Pharm Sci 2009;99:442–54.
[16] Ishii Y, Miyoshi A, Watanabe R, Tsuruda K, Tsuda M, Yamaguchi-Nagamatsu Y, et al. Simultaneous expression of guinea pig UDP-glucuronosyltransferase 2B21 and 2B22 in COS-7 cells enhances UDP-glucuronosyltransferase 2B21-catalyzed morphine 6-glucuronide formation. Mol Pharmacol 2001;60:1040–8.
[17] Ishii Y, Miyoshi A, Maji D, Yamada H, Oguri K. Simultaneous expression of guinea pig UDP-glucuronosyltransferase 2B21 (UGT2B21) and 2B22 in COS-7 cells enhances UGT2B21-catalyzed chloramphenicol glucuronidation. Drug Metab Dispos 2004;32:1057–60.
[18] Ikushiro S-I, Emi Y, Iyanagi T. Protein-protein interactions between UDP-glucuronosyltransferase isozymes in rat hepatic microsomes. Biochemistry 1997;36:7154–61.
[19] Miners JO, Mackenzie PI, Knights KM. The prediction of drug glucuronidation parameters in humans: UDP-glucuronosyltransferase enzyme-selective substrate and inhibitor probes for reaction phenotyping and in vitro–in vivo extrapolation of drug clearance and drug-drug interaction potential. Drug Metab Rev 2010;42:196–208.
[20] Court MH, Krishnaswamy S, Hao Q, Duan SX, Patten CJ, von Moltke LL, et al. Evaluation of 3′-azido-3′-deoxythymidine, morphine and codeine as probe substrates for UDP-glucuronosyltransferase 2B7 (UGT2B7) in human liver microsomes: specificity and influence of the UGT2B7*2 polymorphism. Drug Metab Dispos 2003;31:1125–33.
[21] Stone AN, Mackenzie PI, Galetin A, Houston JB, Miners JO. Isoform selectivity and kinetics of morphine 3- and 6-glucuronidation by human UDP-glucuronosyltransferases: evidence for atypical glucuronidation kinetics by UGT2B7. Drug Metab Dispos 2003;31:1086–9.
[22] Raungrut P, Uchaipichat V, Elliot DJ, Janchawee B, Somogyi AA, Miners JO. In vitro–in vivo extrapolation predicts drug–drug interactions arising from inhibition of codeine glucuronidation by dextropropoxyphene, fluconazole, ketoconazole and methadone in humans. J Pharmacol Exp Ther 2010;334:609–18.
[23] Miners JO, Valente L, Lillywhite KJ, Mackenzie PI, Burchell B, Baguley BC, et al. Preclinical prediction of factors influencing the elimination of 5,6-dimethylxanthenone-4-acetic acid, a new anticancer drug. Cancer Res 1997;57:284–9.
[24] Innocenti F, Iyer L, Ramirez J, Green MD, Ratain MJ. Epirubicin glucuronidation is catalyzed by human UDP-glucuronosyltransferase 2B7. Drug Metab Dispos 2001;29:686–92.
[25] Mano Y, Usui T, Kamimura H. The UDP-glucuronosyltransferase 2B7 isozyme is responsible for gemfibrozil glucuronidation in the human liver. Drug Metab Dispos 2007;35:2040–4.
[26] Jin C-J, Miners JO, Lillywhite KJ, Mackenzie PI. Complementary deoxyribonucleic cloning and expression of a human liver uridine diphosphate glucuronosyltransferase glucuronidating carboxylic acid containing drugs. J Pharmacol Exp Ther 1993;264:475–9.
[27] Bowalgaha K, Elliot DJ, Mackenzie PI, Knights KM, Swedmark S, Miners JO. S-Naproxen and desmethylnaproxen glucuronidation by human liver

microsomes and recombinant human UDP-glucuronosyltransferases (UGT): role of UGT2B7 in the elimination of naproxen. Br J Clin Pharmacol 2005;60:423–33.
[28] Jin C-J, Mackenzie PI, Miners JO. The regio- and stereo-selectivity of C19 and C21 hydroxysteroid glucuronidation by UGT2B7 and UGT2B11. Arch Biochem Biophys 1997;341:207–11.
[29] Bowalgaha K, Elliot DJ, Mackenzie PI, Knights KM, Miners JO. The glucuronidation of (Δ^4-3-keto C19 and C21 hydroxysteroids by human liver microsomal and recombinant UDP-glucuronosyltransferases (UGTs): 6α- and 21-hydroxyprogesterone are selective substrates of UGT2B7. Drug Metab Dispos 2007; 35:363–70.
[30] Knights KM, Winner LK, Elliot DJ, Bowalgaha K, Miners JO. Aldosterone glucuronidation by human liver and kidney microsomes and recombinant UDP-glucuronosyltransferases: inhibition by NSAIDs. Br J Clin Pharmacol 2009;68:402–12.
[31] Lewis BC, Mackenzie PI, Elliot DJ, Burchell B, Bhasker CR, Miners JO. Amino terminal domains of human UDP-glucuronosyltransferases (UGT) 2B7 and 2B15 associated with substrate selectivity and autoactivation. Biochem Pharmacol 2007;73:1463–73.
[32] Uchaipichat V, Mackenzie PI, Guo XH, Gardner-Stephen D, Galetin A, Houston JB, et al. Human UDP-glucuronosyltransferases: isoform selectivity and kinetics of 4-methylumbelliferone and 1-naphthol glucuronidation, effects of organic solvents, and inhibition by diclofenac and probenecid. Drug Metab Dispos 2004;32:413–23.
[33] Uchaipichat V, Galetin A, Houston JB, Mackenzie PI, Williams JA, Miners JO. Kinetic modeling of the interactions between 4-methylumbelliferone, 1-naphthol, and zidovudine glucuronidation by UDP-glucuronosyltransferase 2B7 (UGT2B7) provides evidence for multiple substrate binding and effector sites. Mol Pharmacol 2008;74:1152–62.
[34] Radominska-Pandya A, Bratton SM, Redinbo MR, Miley MJ. The crystal structure of human UDP-glucuronosyltransferase 2B7 C-terminal end is the first mammalian UGT target to be revealed: the significance for human UGTs from both the 1A and 2B families. Drug Metab Rev 2010;42:133–44.
[35] Kerdpin O, Mackenzie PI, Bowalgaha K, Finel M, Miners JO. Influence of N-terminal domain histidine and proline residues on the substrate selectivities of human UDP-glucuronosyltransferase 1A1, 1A6, 1A9, 2B7, and 2B10. Drug Metab Dispos 2009;37:1948–55.
[36] Eddy SR. Profile hidden Markov models. Bioinformatics 1998;14:755–63.
[37] Lewis BC, Mackenzie PI, Miners JO. Comparative homology modeling of human cytochrome P4501A1 (CYP1A1) and confirmation of residues involved in 7-ethoxyresorufin O-deethylation by site-directed mutagenesis and enzyme kinetic analysis. Arch Biochem Biophys 2007;468:58–69.
[38] Powell MJD. Restart procedures for the conjugate gradient method. Math Program 1977;12:241–54.
[39] Kini RM. Proline brackets and identification of potential functional sites in proteins: toxins to therapeutics. Toxicon 1998;36:1659–70.
[40] Donald JE, Kulp DW, DeGrado WF. Salt bridges: geometrically specific, designable interactions. Proteins Struct Funct Bioinform 2011;79:898–915.
[41] Hunter CA, Sanders JKM. The nature of pi–pi interactions. J Am Chem Soc 1990;112:5525–34.
[42] Pal D, Chakrabarti P. Non-hydrogen bond interactions involving the methionine sulfur atom. J Biomol Struct Dyn 2001;19:115–28.
[43] Zhou J, Tracy TS, Remmel R. Glucuronidation of dihydrotestosterone and transandrosterone by recombinant UDP-glucuronosyltransferase (UGT) 1A4: evidence for multiple UGT1A4 aglycone binding sites. Drug Metab Dispos 2010;38:431–40.
[44] Jones S, Thornton JM. Principles of protein–protein interactions. Proc Natl Acad Sci (USA) 1996;93:13–20.
[45] Jones S, Thornton JM. Protein–protein interactions – a review of protein dimer structures. Prog Biophys Mol Biol 1995;63:31–65.
[46] Young L, Jernigan RL, Covell DG. A role for surface hydrophobicity in protein–protein recognition. Protein Sci 1994;3:717–29.
[47] Janin J, Chothia C. The structure of protein–protein recognition sites. J Biol Chem 1990;265:16027–30.
[48] Chothia C, Janin J. Principles of protein–protein recognition. Nature 1975;256: 705–8.
[49] Neet KE, Timm DE. Conformational stability of dimeric proteins – quantitative studies by equilibrium denaturation. Protein Sci 1994;3:2167–74.
[50] Xu D, Tsai CJ, Nussinov R. Mechanism and evolution of protein dimerization. Protein Sci 1998;7:533–44.